Journal of Materials Chemistry A

Polysulfide entrapment and retardation in gel electrolyte Li-S batteries: experiments and modeling

Journal:	*Journal of Materials Chemistry A*
Manuscript ID	TA-ART-12-2019-014234.R1
Article Type:	Paper
Date Submitted by the Author:	28-Jan-2020
Complete List of Authors:	Shebert, George; Cornell University, Chemical and Biomolecular Engineering Zamani, Somayeh; Cornell University, Yi, Caspar; Cornell University Joo, Yong Lak; Cornell University, Chemical and Biomolecular Engineering

Polysulfide entrapment and retardation in gel electrolyte Li-S batteries: experiments and modeling

George L. Shebert[+], Somayeh Zamani[+], Caspar Yi, and Yong Lak Joo*

Robert Frederick Smith School of Chemical and Biomolecular Engineering, Cornell University, Ithaca, NY 14853 USA

*Corresponding author: ylj2@cornell.edu

[+]Co-first authors

Keywords: Lithium-sulfur battery discharge, gel electrolyte, numerical simulation, mass transport limitation, Diffusivity

Abstract

Gelling the electrolyte in Lithium-Sulfur (Li-S) batteries provided advantages in terms of safety and mitigating polysulfide shuttle leading to reduced side reaction and dendrite growth on the anode side. Organic and ceramic crosslinkers were used to improve the entrapment of polysulfides preventing them from shuttling to the anode side. However, it is still far from performing on par with liquid electrolyte in terms of raw capacity. The discharge curves exhibited extended first plateau for the gel electrolyte batteries compared to liquid electrolyte, denoting that the polysulfides are better trapped in the gel system. Yet, the conversion of the soluble polysulfides into insoluble polysulfides, the second plateau was retarded. Qualitative and quantitative analysis of the polysulfide diffusion in the liquid electrolyte and gel electrolyte systems were conducted to predict the relative diffusivity ratio between the liquid electrolyte and gel electrolyte for the simulation. To probe the end of discharge, where the mass transport in gel electrolyte appears to be too slow, a modified discharge procedure was used where the cell is first paused after discharge and then discharged a second time before recharging normally. Coin cell tests for two gel electrolytes in addition to liquid electrolyte show up to 7% capacity recovered after the pause, which indicates that diffusion of species during the pause is responsible for the failure recovery. Additionally, recovery is higher for gel electrolytes compared to liquid, for higher C-rates, and for longer pause times. To better understand this behavior, a Li-S numerical model with mass transport limited reactions was used

to examine the polysulfide diffusion coefficients expected in different electrolyte systems. The model is able to reproduce the trends seen in experiment and yields higher recovery for smaller Li_2S_4 diffusion coefficients, suggesting that insufficient Li_2S_4 mass transport is responsible for failure at end of discharge. By identifying the effect of gel electrolyte on the state of the battery during discharge using both experimental and simulation methods, this work is a step towards leveraging the advantages of gel electrolytes and mitigating their weaknesses.

1. Introduction

As interest in renewable energy grows and demand for electric vehicles strengthens, it is crucial for energy storage technology to improve beyond the currently used lithium-ion (Li-ion) batteries.[1] Lithium-sulfur batteries (Li-S) are one of the most promising battery candidates to replace Li-ion batteries due to their high theoretical specific energy of 2510 W H kg^{-1}.[2] In addition, the low cost and plentiful supply of sulfur is preferred to the expensive and relatively scarce cobalt frequently used in Li-ion battery cathodes. However, Li-S batteries still suffer from a number of challenges that limit their viability. First, intermediate lithium polysulfide species formed during the electrochemical conversion of sulfur have high solubility in the battery electrolyte, allowing movement away from reaction sites in the cathode and leading to side reactions at the anode.[3–7] Second, lithium sulfide discharge products are insulating, requiring the use of conductive carbon host materials and limiting the sulfur loading and energy density of the battery.[8–10] The sulfur to lithium sulfide conversion during discharge also involves a 79% volume expansion which can damage the cathode structure over many cycles.[11,12] Li-S research has focused in large part in developing strategies that reduce or eliminate these challenges.

To limit the movement of polysulfide out of the cathode, many researchers have developed carbon or other materials that can trap or adsorb the polysulfides. These materials have shown improved cycle performance and capacity, but can add significant costs due to complex material synthesis and sulfur impregnation processes.[13,14] Another approach is to use gel polymer electrolyte (GPE) or gelled liquid electrolyte (GE) instead of the traditional liquid electrolyte (LE), which has already proven successful in Li-ion battery research.[15–17] By trapping solvent molecules in a polymerized or crosslinked gel network, the transport and solubility of polysulfides can be suppressed. Gel electrolyte also reduces flammability and suppresses the formation of dendrites on the lithium metal surface that can puncture the battery separator, which are crucial safety concerns.[18] Previous work has shown promising results in the

application of gel electrolyte to Li-S systems. Natarajan used a polyethylene oxide GPE with plasticizer additives to improve the gel's ionic conductivity and showed preliminary Li-S results.[19] Chen et al. used a polyethylene oxide GPE which enabled lower electrolyte to sulfur ratios, and they identified passivation of the cathode as the failure mechanism.[20] Liu et al. used a pentaerythritol tetraacrylate GPE which limited polysulfide diffusion, improved interfacial contact, and showed better rate capability than liquid electrolytes.[21]

Gelling the electrolyte, lead to improved safety, reduced dendrite growth on the anode, and mitigated polysulfide diffusion. Yet, the capacity of the gel electrolyte batteries was lower or comparable with that of liquid electrolyte. Moreover, the complexity of the Li-S system makes fundamental understanding difficult with experimental methods alone. Li-S numerical simulations have aided Li-S research by demonstrating good experimental agreement and proposing mechanisms for behavior observed in experiment without the need for complex characterization methods. Kumaresan et al. first proposed a 1-dimensional + time Li-S simulation which showed that the Li-S discharge curve could be accurately represented by a series of five sulfur reactions in combination with dissolution and precipitation effects.[22] More recently, simulations have attempted to address the mechanism of cell failure at the end of discharge. Ren et al. proposed a nucleation and passivation mechanism where insulating lithium sulfide precipitates onto the carbon cathode during discharge and eventually covers all of the surface area, resulting in no further ability to perform electrochemical reactions.[23] This has been disputed by Zhang et al., whose experiments and simulations support a mass transport limited mechanism.[24]

For the case of gel electrolytes, no simulations have yet attempted to model the Li-S battery performance. As gel electrolytes further restrict the movement of lithium ions and polysulfides, mass transport limitations that limit discharge capacity may become even more pronounced. In this paper, we use a combination of experiments and simulations in order to investigate the effect of electrolyte choice on fundamental Li-S behavior. We first compare experimental results for liquid electrolyte and gelled liquid electrolyte systems. To probe the end of discharge behavior, we use a specialized discharge method where the cell discharges until 1.8V, pauses for a chosen amount of time, and then attempts to continue discharge. By examining the capacity recovered after the pause, the reason for the cell's original failure at discharge can be elucidated. We then use numerical simulation with the same pause discharge procedure to explain and gain further insight into the experimental results. In our simulations, we specifically focus on the effect of slower polysulfide diffusion caused by the gelled electrolyte by directly varying the Li_2S_4 diffusion coefficient to obtain the calculated relative diffusivity based on the experimental

diffusion test. Understanding the end-of-discharge behavior for gel and liquid electrolyte systems is crucial in the effort to improve battery capacity through rational cathode and electrolyte design.

2. Li-S coin cell methods and materials

Sulfur powder (S, 1.5 g) was ground with Ketjen Black EC600JD (KB, 0.5g, AkzoNobel) to get a 75:25 S:KB mixture. Then the mixture was heat treated at 155°C for at least 12 h to ensure sulfur impregnation into the porous KB particles.[31] The active material S/KB was then thoroughly mixed for 3h with Super C-65 (MTI Corp.) and the binder polyvinylidene fluoride (PVDF, Aldrich) in N-methyl-2-pyrrolidone (NMP, BDH), in the weight ratio of 70:20:10, respectively. The slurry was cast onto aluminum foil using doctor's blade and the sheets were dried in a fume hood at room temperature overnight followed by heat treatment at 55°C oven. The total thickness of aluminum + cathode was 54 microns, and sulfur areal loading was around 1 mg cm^{-2} for all cells.

All cells (2032 type) were assembled in an argon filled glovebox. A typical cell consisted of a lithium metal disc (Alfa Aesar) as anode, a S/KB slurry cast as cathode (1mg/cm2), and a Celgard 2400 separator (25 micron thickness). The electrolyte was 1M (LiTFSI, Sigma-Aldrich) and 0.1M $LiNO_3$ (Sigma-Aldrich) in a 1:1 volume ratio of dioxolane (DOL, Sigma-Aldrich) and dimethoxyethane (DME, Sigma-Aldrich).[32] 10 wt% trimethylolpropane trimethacrylate (TPTA, Sigma-Aldrich) as crosslinker along with 1wt% azobisisobutyronitrile (AIBN, Sigma-Aldrich) as initiator was added to the abovementioned electrolyte for TPTA gel electrolyte cells and cells were assembled after complete dissolution of the components. 5wt% polyhedral oligomeric silsesquioxane methacrylate (POSS-MA, Hybrid Plastic), a cage-like crosslinker, and 1wt% AIBN were used instead for the POSS-MA gel electrolyte cells. A 30 minutes heat treatment at 70°C was applied to the cells after 3h of rest to gel the electrolyte *in situ*. The electrolyte to sulfur ratio was 20µl per mg of sulfur in all the liquid and gel electrolyte batteries.

Galvanostatic charge-discharge measurements were performed using a MTI Corporation battery cycler at room temperature. A discharge procedure was used where the cell is first discharged to 1.8V, then paused after discharge, and lastly then discharged a second time to 1.8V before recharging normally. The tests were run with 6 cycles at the same C-rate, with the first 3 cycles having no pause and the second 3 cycles having a pause. The 6 cycles were repeated at successively higher C-rates from 0.1C to 1.0C.

Field Emission Scanning Electron Microscope (FESEM, LEO 1550) at an accelerating voltage of 2kV was used to analyze the dendrite growth on the anode surface.

3. Polysulfide diffusion experiment

3.1. Li_2S_6 solution

In an argon filled glovebox, elemental sulfur (S) and lithium sulfide (Li_2S) were mixed in a 5:1 molar ratio. The mixture was then added to a 1:1 volume ratio of DME and DOL to form a 0.2M lithium sulfide solution (reactant product Li_2S_6). The solution was then heated on a hot plate for 70 °C for 24 hours to produce a deep orange/brown polysulfide solution.

3.2. Qualitative diffusion test

The diffusion setup comprised of two compartments of cathode and anode with a separator in between the chambers. The "cathode" compartment was filled with the polysulfide mixture and the "anode" side was filled with 1:1 DME/DOL. A stir bar was used in each side to continuously homogenize the solution. Photos were taken immediately after pouring the polysulfide mixture on the "cathode" side in order to qualitatively determine the amount of polysulfides that diffused into the anode side. Photos were taken up to 8 hours.

3.3. Quantifying the Li_2S_6 diffusion rate

UV-Vis Spectroscopy (Cary 5000 UV-vis near-infrared spectrophotometer) was used to quantify the amount of polysulfide diffused to the anode side. Polysulfide samples (2 ml) were taken at time intervals of 2, 5, 7.5, 10, 15, and 20 min. The aliquots were transferred to UV-Vis in a quartz cuvette and analyzed in a wavelength range from 200 to 800 nm. Calibration curve was obtained by measuring the absorbance of diluted polysulfide solutions. Starting from a known 0.2M concentration of Li_2S_6, 100 µL was diluted with 9.9 mL of DME:DOL and subsequently diluted to achieve various concentrations. A linear and stable relationship was observed at 420 nm for Li_2S_6. The Diffusion molar flux equation was used to calculate the relative diffusivity of Celgard 2400 to TPTA-crosslinked Celgard 2400 (Supporting information, Fig. S1 and S4).

3.4. Flammability test

Flammability of the separator materials in LE and GE batteries was tested. Celgard separators were soaked in liquid electrolyte (LE) and TPTA-included liquid electrolyte (GE), followed by heat treatment of the GE separators. The separators were then exposed to three second intervals of lightening and photos were taken after each exposure.

4. Theoretical model

4.1. Electrochemical and precipitation reactions

During discharge, elemental sulfur (S_8) is converted into successive lithium polysulfides (Li_2S_x) until finally forming lithium sulfide (Li_2S) The full diversity of lithium polysulfides that may exist in the battery is not fully understood; however, it has been shown by previous models that the characteristic discharge behavior can be captured with a limited subset of electrochemical reactions.[22] In our model, we use four polysulfide electrochemical reactions and consider the dissolution of S_8 and the precipitation of Li_2S as separate reactions. The remaining polysulfide species are assumed have negligible precipitation, which is supported by experimental work.[25] The electrochemical and precipitation reactions occurring at the cathode are listed below:

$$S_8^{(s)} \rightleftharpoons S_8^{(l)}$$

$$S_8^{(l)} + e^- \rightleftharpoons S_8^{2-}$$

$$\frac{3}{2}S_8^{2-} + e^- \rightleftharpoons 2S_6^{2-}$$

$$S_6^{2-} + e^- \rightleftharpoons \frac{3}{2}S_4^{2-}$$

$$\frac{1}{3}S_4^{2-} + e^- \rightleftharpoons \frac{4}{3}S^{2-}$$

$$S^{2-} + 2Li^+ \rightleftharpoons Li_2S^{(s)}$$

The first two reaction occur at the beginning of discharge in the first plateau region of the typical Li-S discharge curve. The third and fourth reactions then occur in the downward sloping region after the first plateau once the elemental sulfur is consumed, and the fifth and sixth reactions occur during the second plateau region once the longer chain polysulfides are consumed.

At the anode, lithium ions are produced at a rate determined by the applied current *I* with the following reaction:

$$Li_s \rightleftharpoons Li^+ + e^-$$

The lithium salt anion is denoted as A^-, which would be bis(trifluoromethane sulfonyl) imide in our electrolytes. As solid species are dissolved or precipitated, their volume fractions ε_i change with time *t* according to Eq. 1:

$$\frac{\partial \varepsilon_i}{\partial t} = \frac{M_i}{\rho_i}\sum_m a_s v_{i,m} r_m \qquad (1)$$

where M_i is molecular weight of solid species *i*, ρ_i is the density, a_s is the specific surface area, $v_{i,m}$ is the stoichiometric coefficient for species *i* in reaction m, r_m is the reaction rate of reaction m for the two precipitation reactions (reactions 1 and 6 in Table 1). We use subscript *i* to denote species and subscript *m* to denote reactions Values of density and molecular weight are listed in Table 1, and stoichiometric coefficients are taken from the coefficients in the reactions with reactant side values being negative. Values of surface area and other structural parameters can be found in Table 2. The volume fraction of electrolyte, ε, is calculated directly from volume fraction of all precipitated species plus the volume fraction of carbon subtracted from 1, seen in Eq. 2:

$$\varepsilon = 1 - \varepsilon_c - \sum \varepsilon_i \qquad (2)$$

where ε_c is the volume fraction of solid carbon or separator in the cell. Reaction rates for each electrochemical cathode reaction (reactions 2-5) are defined by a modified mass transport limited Butler-Volmer equation in Eq. 3:

$$r_m = k_m (a_{re} a_{prod})^{0.5} \left(\left(1 - \frac{r_m}{r_{l,c}}\right) e^{-\frac{1}{2RT}\Delta\mu_m} - \left(1 - \frac{r_m}{r_{l,a}}\right) e^{\frac{1}{2RT}\Delta\mu_m} \right) \qquad (3)$$

where k_m is a reaction constant, $r_{l,c}$ is a limiting reactino rate, R is the gas constant, T is temperature, and $\Delta\mu_m$ is the change in chemical potential for reaction *m.* It should be noted that r_m is scaled by the cathode surface area with units of mol $m^{-2}s^{-1}$. a_{re} and a_{prod} represent the activities of reactants and products respectively, as used in Danner et. al.[27] Symmetry and acitivity coefficients were assumed to be 0.5 and 1 respectively. The $\left(1 - \frac{r_m}{r_{l,c}}\right)$ term represents a mass transport limitation which reduces the reaction rate as the reaction rates approach some limit.[28] This limit represents the maximum rate at which reactants can be supplied to reaction sites in the cathode. Above this rate it is not possible for the cell meet the demanded external current. Excluding the mass transport limitation, this form of the Butler-Volmer equation was taken from Bazant.[26,27] The limiting reaction rate is given by Eq. 4:

$$r_{l,c} = a_{mtl}\left(c_{Li^+}\left(c_{S_4^{2-}} + c_{S_6^{2-}}\right)\right)\left(1 - \frac{\varepsilon_{Li_2S}}{\varepsilon_{max}}\right)^{b_{mtl}} \qquad (4)$$

where a_{mtl} and b_{mtl} are fitting parameters chosen to match experimental data and c_i is concentration. The limiting reaction rate for the reverse reaction $r_{l,a}$is assumed to be the same as $r_{l,c}$. This term assumes that the maximum mass transport rate to reaction sites will decrease as the cathode is clogged with solid deposits and as the concentrations of reactants decreases in the bulk. The form of this limitation is similar to that used previously by Zhang et al.[24]

For electrochemical reaction, the change in chemical potential and equilibrium voltage is given in Eqs. 5 and 6 [26,27]:

$$\Delta\mu_m = n_m F(\phi_{cathode} - U_{eq,m}) \quad (5)$$

$$U_{eq,m} = U_{eq0,m} + RTln(\frac{a_{re}}{a_{prod}}) \quad (6)$$

where n_m is the number of electrons per reaction, F is the Faraday constant, $\phi_{cathode}$ is the voltage of the carbon cathode, $U_{eq,m}$ is the open circuit potential for reaction *m*, and $U_{eq0,m}$is the open circuit potential at reference conditions. Sulfur (S_8) and lithium sulfide (Li_2S) undergo precipitation/dissolution reactions with $\Delta\mu_m$ given by Equation 7 instead:

$$\Delta\mu_m = RTln(K_{sp,m}\frac{a_{prod}}{a_{re}}) \quad (7)$$

where $K_{sp,m}$ is the solubility product for precipitation reaction *m*. Parameters used in reactions are listed in Table 1.

4.2 Governing equation and mass transport

Changes in concentration of each species depend on mass transport and reaction terms, as shown in Eq. 8:

$$\frac{\partial}{\partial t}(\varepsilon c_i) = -\frac{\partial N_i}{\partial z} + \sum_m a_s v_{i,m} r_m \quad (8)$$

where N_i is the mass flux of species *i* and *z* is the distance dimension between anode and cathode. Our model assumes that transport is purely diffusive due to the computational difficulty of including migration with the inner-outer discretization approach (section 3.4). This assumption has been also used by a previous model with a similar discretization scheme.[29] With this assumption, the flux is given Fick's Law in Eq. 9:

$$N_i = -D_{eff,i}\frac{\partial c_i}{\partial z} \quad (9)$$

where $D_{eff,i}$ is the effective diffusion coefficient. This value is found by adjusted based on porosity using the Bruggeman correlation in Eq. 10 [22,30]:

$$D_{eff,i} = D_{0,i}\,\varepsilon^{\beta} \quad (10)$$

where $D_{0,i}$ is the bulk diffusion coefficient and β is the Bruggeman coefficient.

4.3 Cell voltages

The total current I, which is determined externally by the rate of discharge, can be found by integrating all electrochemical reactions over the total cell length l_c:

$$I = \int_0^{l_c}(\sum_m - n_m F a_{s,m} v_{i,m} r_m)dz \quad (11)$$

Eq. 11 can be solved numerically to find $\phi_{cathode}$ using I and the current concentrations of species. The total cell voltage can be found from the difference of cathode and anode voltages:

$$V_{cell} = \phi_{cathode} - \phi_{anode} \quad (12)$$

The anode voltage is estimated in Eq. 13 using Nernst's equation for lithium metal oxidation[29]:

$$\phi_{anode} = \frac{RT}{F} ln(\frac{c_{Li+,anode}}{c_{Li+,ref}}) \quad (13)$$

where $c_{Li+,ref}$is the reference concentration for lithium ion.

4.4 Cell structure and numerical implementation

We use a 1-dimensional + time numerical approach which models the Li-S full cell. Due to symmetry in the cell structure, we assume that only the dimension separating the anode and the cathode is relevant. The governing equations are discretized using Finite Difference Method to form N=11 segments and solved in Matlab using the ode15s stiff solver. Initial conditions for concentration and volume fraction are listed in Table 2. The cell structure is characterized by its porosity, specific surface area, and Bruggeman coefficient, with parameters given in Table 3. In order to represent the spherical nature of carbon particles, we construct inner boxes in the cathode region that are connected to a single outer box, shown in Fig. 1, which are separated from each other by distance l_{io}. The inner box represents the interior of a porous carbon particle, and the outer box represents the exterior of the carbon particle and the surrounding electrolyte. Therefore, species must first travel through the outer boxes and then may travel from an outer box in the cathode into an inner box. The inner boxes have high surface area and tortuosity

reflecting the nm-sized pores present in the Ketjen Black carbon used in our experiments. Solid sulfur exists only in the inner cathode region at time 0 to reflect impregnation into porous carbon material. A related discretization approach was published previously by Thangeval et al.[29]

Parameters for the model are taken from experimental sources where possible, but many parameters are not accurately known. In these cases, we assume parameters based on agreement between simulation discharge curves and previously published experimental discharge curves.[23]

5. Results and Discussion

5.1. Effect of gel electrolyte on safety and dendrite growth

TPTA as an organic crosslinker and POSS-MA as a ceramic-based crosslinker were used to gel the electrolyte with the goal of safer battery with less dendrite growth and improved entrapment of polysulfides. The chemical structure and FT-IR images of the crosslinkers are presented in Fig. S2.

Celgard (2400), LE-soaked Celgard, TPTA-crosslinked Celgard, and POSS-crosslinked Celgard were exposed to the flammability test. It was expected that gel electrolytes by trapping solvent molecules will extend the resistance to flammability and in the POSS_MA case, due to its ceramic characteristics, the resistance will even be longer. Fig. 2 illustrates the summary of the flammability test and more detailed images are presented in Fig S3. Celgard when soaked in liquid electrolyte was prone to flame in a few exposures and shriveled up. Crosslinking the liquid electrolyte on Celgard on the other hand, retarded the flammability of the separator and the integrity of the separator was maintained for a considerably longer time. POSS-crosslinked Celgard outperformed the organic TPTA-crosslinked Celgard, as expected and it exhibited some degree of self-extinguishing properties (Fig. S3). Furthermore, Li metal anode after cycling was analyzed by SEM in an attempt to compare the aforementioned dendrite growth in the liquid electrolyte versus gel electrolyte batteries. The exhibited smoother surface in the gel electrolyte anode (Fig. 3) can be an indicative of reduced side reactions on the anode due to less diffusion of polysulfides towards the anode.

5.2. Electrochemical performance of Gel electrolyte vs liquid electrolyte batteries

Coin cells with a slurry cast cathode, lithium metal anode, and a Celgard 2400 separator were fabricated to investigate the electrochemical performance of the gel electrolyte and liquid electrolyte batteries. The LiTFSI/$LiNo_3$ electrolyte was crosslinked by TPTA or POSS-MA as 10 wt% and 5wt%, respectively in the gel electrolyte cells. Both gel electrolyte batteries exhibited improved rate capability at high 2C rate (Fig. 4a).

POSS-MA gel electrolyte performed better than TPTA in general, which is likely due to its cage like structure that helps better trap the polysulfides.

The charge/discharge profile of the batteries presented in Fig. 4b, reveal that the capacity retention of the battery is improved by gelling the electrolyte however, the raw capacity of the gel electrolyte system is in fact, lower than that of liquid electrolyte. To better understand the reason for the lower capacity of the gel electrolyte batteries, we further focused on the first discharge curve in all the three cases (Fig. 2c). The discharge curves clearly show that the first plateau which is related to the formation of polysulfides and sulfur utilization, was extended by gelling the electrolyte with either the crosslinkers, conversely, the second plateau that is related to the conversion of the soluble polysulfides into insoluble ones is shortened for the two gel systems. This indicates that either the mass transport of the reactants which are likely the Li_2S_4 and Li_2S_6, is extensively retarded or the reaction sites are passivated by deposition of insoluble lithium sulfides.

To benefit from such advantages of the gel electrolyte there is still the need for further understanding of what happens at the end of discharge. The “discharge with pause” was carefully designed to shed more light on the failure mechanism that lead to the difference in the capacities between the liquid and gel electrolyte.

5.3. Qualitative and quantitative analysis of diffusion of Li_2S_6 to the anode

Fig. 5 provides time lapse photos of the diffusion test that was performed under Ar atmosphere to resemble the diffusion of polysulfide species in the gel electrolyte versus liquid electrolyte Li-S batteries. The experiment was performed in a diffusion cell where polysulfide injected to one side and the transport through a normal separator and gelled separator was compared over time. Images clearly reveal the slowdown of diffusion of polysulfides through a gelled separator compared to the liquid electrolyte filled separator. The diffusion slowdown is expected to be even greater when considering a full Li-S cell that has separator, cathode, and anode all filled with gel electrolyte instead of only the separator considered in this experiment.

In an attempt to quantify the diffusion of polysulfides through the separator, UV-Vis spectroscopy was used. Keeping in mind that obtaining absorbance of standard solutions was only possible for low concentrations due to the UV absorbance limitations, relative diffusivity of Celgard to TPTA gelled separator was calculated based on Eq S1 and S2 and it was equal to ~23.9 (Supporting information, Fig S4). however the apparent diffusivity (based on the photos) was lower than the calculated value.

Numerical simulation was conducted based on the calculated effective diffusivity to explain and gain insight into the mechanism of failure.

5.4. Effect of electrolyte and discharge rate on capacity recovered after pause

In order to investigate the behavior of Li-S cells at the end of discharge, we used a special discharge method in both experiment and simulation tests. This consisted of a normal discharge to the 1.8V lower cutoff, followed by a pause of variable length with zero current, followed lastly by a second discharge at the same rate as the first. At the end of the first discharge, we expect one of three scenarios to occur: first, all polysulfides have been consumed in the entire battery so no more reactants are available; second, insulating lithium sulfide deposits have fully passivated the cathode allowing no further transfer of electrons; or third, polysulfide or lithium ion reactants cannot reach reaction sites fast enough due to a mass transport limitation. Only in the third scenario would it be possible to see additional capacity during the second discharge after the pause.

The discharge curves for the liquid electrolyte and TPTA gel electrolyte systems for a 1 hour pause are shown in Figs. 6a and 6b. Capacities are scaled by grams of sulfur used in the cell. The 1 hour pause occurs after the voltage reaches 1.8V the first time in the plot. A comparison of Figs. 6a and 6b shows that liquid electrolyte has better performance and rate capability, which is due to the worsened ionic conductivity in the gelled system. After the pause, both liquid and gel electrolytes show recovered capacity, which demonstrates that some change happened within the cell during the 1 hour pause. The fact that any capacity is recovered suggests that passivation mechanisms are not the sole cause of discharge failure in these cells.[23] If passivation caused the discharge failure, we would expect to see little to no capacity recovered after pause, so a more likely explanation is that at the end of discharge the cell faces a mass transport limitation.[24] Both gel and liquid electrolytes also show increased capacity after pause as the C-rate increases, which further suggests that mass transport plays an important role at the end of discharge. Similar results were also observed for the POSS-MA gel system, shown in Fig. S5 (Supporting Information). Mass transport in the cathode is affected by the lithium sulfide deposition, which reduces porosity and constricts diffusion pathways, but will also be affected by the diffusion of species, raising questions regarding the mechanism behind the recovery and the effect of the gel electrolyte.

Using the numerical model presented in section 4, we perform the same discharge procedure with 1 hour pause in order to investigate the behavior observed in experiment. As the 2nd plateau discharge region

involves the conversion of Li_2S_4 and there is evidence of mass transport limitation, we use the model to investigate the effect of Li_2S_4 diffusion coefficient on the end of discharge performance. Fig. 7 shows the simulation results for multiple C-rates and two Li_2S_4 diffusion coefficients. The numerical model reproduces the characteristic shape of the Li-S discharge profile, and its capacities are comparable with those predicted by Andrei et al.[23] Due to the assumptions in the model such as perfect carbon conductivity, full utilization of solid sulfur, and no shuttle effect, the model represents a more ideal case with higher discharge capacities compared to experiment. The simulation results show similar trends as experiment, with some capacity recovered after pause and increasing recovery at higher C-rates. In addition, with slower Li_2S_4 diffusion, the simulation predicts larger capacity recovery after pause, which corresponds to the gel system where diffusion is more difficult. A relative diffusivity of liquid electrolyte to TPTA of ~20 was perfectly consistent with the calculated relative diffusivity based on the experiments.

The trends in C-rate and Li_2S_4 diffusion can be explained by considering the transport of Li_2S_4 during cell discharge. Between the capacities of around 300 to 400 $mAhg^{-1}$ in Fig. 7, Li_2S_4 is being produced at the cathode. This creates a concentration gradient from the cathode to anode leading to diffusion of Li_2S_4 away from the cathode inner regions to the cathode outer regions and separator. Later, as Li_2S_4 is consumed in the 2^{nd} plateau region of Fig. 7 with capacities greater than 400 $mAhg^{-1}$, Li_2S_4 that previously drifted away from the cathode begins to diffuse back. Based on the C-rate, which controls the amount of time for the process to occur, and the diffusion coefficient, differing amounts of Li_2S_4 may remain in the cell. The subsequent pause provides additional time for Li_2S_4 to diffuse back to the cathode where it can be converted to yield additional capacity once the second discharge begins. Therefore, at higher C-rates, Li_2S_4 has less time to return to the cathode during the 2^{nd} plateau, leading to greater benefits after the pause. Likewise, slower diffusion in Fig. 7b results in greater recovery after pause than in Fig. 7a as fewer polysulfides were able to return to the cathode during the first discharge.

To evaluate this explanation, we compared the experiment and model predictions. To do this we calculated the percent recovery after pause, which is equal to the capacity gained during the second discharge divided by the total discharge capacity. The percent recoveries for simulation and experiment for 1 hour pause time are shown in Fig. 8. For experiment, the pause recovery presented is an average over three identical, consecutive cycles. Although the model underpredicts the percent capacity, likely due to the higher total capacity predicted in the model, the simulation and experiment show similar increasing recovery with C-rate. Also, the gel electrolyte percent recovery is higher than the liquid case.

By reducing the Li_2S_4 diffusion coefficient, the simulation predicts a similar increase in recovery due to the inability of Li_2S_4 to return to the cathode fast enough near the end of discharge.

While our model shows that it is possible to explain the experimental results by varying Li_2S_4 mass transport, it is difficult to separate the effect of lithium ion transport in the experimental results. To investigate lithium ion effects further, we tested liquid and gel systems with 1.5M LiTFSI instead of 1.0M. If the capacity recovery in experiment is due to a lithium ion mass transport limitation instead of Li_2S_4, we would expect to see some change in total capacity and recovered capacity with more plentiful lithium ions. In Fig. S6 (Supporting Information), the 1.5M LiTFSI results were nearly identical to the results in Fig. 6a using 1.0M LiTFSI, indicating that lithium ion transport limitations cannot explain the capacity recovery effect.

Another point which should be considered is the effect of migration on the lithium and polysulfide ions. The numerical model does not include the effects of migration, which limits the simulation to only investigating diffusion driven effects. However, if migration was included, it would increase the movement of lithium ions towards the cathode and polysulfide ions toward the anode during discharge. Therefore, migration would decrease lithium ion mass transport problems and increase polysulfide mass transport problems compared to only considering diffusion.

5.5. Effect of pause time on capacity recovered after pause

The discharge with pause experiments and simulations were performed for pause durations between 5 minutes and 2 hours duration to investigate the time scale of the capacity recovery mechanism. The results for TPTA gel and simulation are shown in Figs. 9a and 9b, respectively. Similar results for liquid electrolyte and POSS-MA gel can be found in Fig. S7. In Fig. 9a, all pause times show similar increases with C-rate as was observed for the 1 hour tests discussed previously. In addition, longer pause times generally cause an increase in percent recovery due to the increased time provided for polysulfides to return to exhausted cathode reaction sites. In Fig. 9b, this mechanism is confirmed by simulations with varying pause times that show similar trends, although the model underestimates the recovery for long pauses with low C-rate. This is likely due to the difference in total capacity between experiments and simulation influencing the percent capacity metric. It also suggests that in addition to diffusion, there is a longer time scale process occurring during discharge and pause. It is expected that given enough time, gains from diffusion should reach a maximum value due to equilibration of the concentration gradient. The improving recovery in experiment with longer pause suggests that there could be a slow release of polysulfides

trapped in the separator or gel electrolyte that is not included in the simulation model. Another possibility is gradual adsorption of polysulfides into the carbon cathode.

Surprisingly, even a short 5 minute pause is sufficient to recover approximately 1-4% capacity in the TPTA system. The 5 minute pause is quite short in comparison to the total discharge time of 10 hours at 0.1C or 1 hour at 1C. However, it is important to note that mass transport limitations will not come into effect until near the end of discharge when there is large deposits of lithium sulfide in the cathode and low Li_2S_4 concentrations, as modeled by Eq. 4. The increasing recovery at longer times shows that the process of Li_2S_4 returning to the cathode has only partially completed at short times. As the recovery during pause is driven by diffusion, less marginal improvement is expected at long pause times where the diffusion gradients have become less steep. This explains why much of the recovery occurs in the first 5 minutes when the diffusion gradients are steepest. The results in Figs. 9a and 9b further demonstrate that the pause recovery is driven by a mass transport mechanism with a time scale on the order of hours.

5.6. Cell voltage after pause

Referring to Fig. 6a and Fig. 6b, the voltage immediately after the pause (2.1V-1.97V for different C-rates, TPTA) is higher than the voltage seen in the plateau region before the pause (2.08V to 1.89V). This is true for all C-rates and electrolytes but becomes more apparent at 0.5C and 1.0C. Although the voltage after the pause rapidly declines until 1.8V, a notable amount of capacity is produced at these higher voltages. This suggests that higher order polysulfide reactions could be taking place after pause, as they react at a higher open circuit voltage. The initial discharge voltages after pause are the same as corresponding voltages earlier during discharge when Li_2S_6 was being converted into Li_2S_4. Therefore, we performed a modified simulation where Li_2S_6 reactions were artificially disabled after the pause. The results are shown in Fig. 10. Compared to the voltage profiles after pause in Fig. 7a and Fig. 7b, the simulation with Li_2S_6 reactions disabled after pause yields recovered capacity at a much lower voltage. This suggests that Li_2S_6 reactions are occurring after the pause and can explain the results seen in Fig. 6. We propose that although much of the Li_2S_6 is consumed much earlier during discharge, some diffuses away from the cathode. This Li_2S_6 then gradually returns while the cell is in the plateau region and is instantly consumed alongside the predominant Li_2S_4 species due to its reaction having a higher open circuit voltage. During the pause, Li_2S_6 is able to return and begins to accumulate instead of instantly being consumed. Then, when the pause ends, the Li_2S_6 is consumed at higher voltage followed by the Li_2S_4 at lower voltage, leading to the observed behavior. It is important to note that because the simulation includes a subset of the true polysulfide species present in experiment, it can only provide an approximation of which species is present after

pause. It is likely that the species present in experiment are not only Li_2S_6 but a mixture of similar polysulfides like Li_2S_5 and Li_2S_7 as well.

6. Conclusions

In summary, we have demonstrated that gelling the electrolyte by organic and ceramic crosslinkers brings improved safety, reduced dendrite growth and mitigated polysulfide shuttle. According to the first discharge curves, gel electrolyte led to improved entrapment of the polysulfides in one hand, illustrated as extended first plateau and retarded conversion of soluble polysulfides into insoluble polysulfides in the other hand, shown as shorter second plateau. The "discharge with pause" test was carefully designed to further our understanding on the mechanism of the failure in the liquid and gel electrolyte. By pausing after discharge, additional capacity can be recovered for both liquid and gel systems. The recovery mechanism was explored using numerical simulation and determined to be related to mass transport limitations as Li_2S_4 diffusion to and from the cathode during discharge. Due to the slower diffusion in the gel electrolyte system compared to liquid, increased percent capacities were recovered. In addition, the higher voltages obtained after pause were proposed to be due to residual Li_2S_6 species still present in the cell at the end of discharge. These results suggest that Li-S battery discharge capacity can be improved by either limiting polysulfide escape from the cathode or speeding its return to the cathode, especially for gel electrolyte systems. This agrees with numerous experimental works that have shown improvements by limiting polysulfide diffusion.[33–39] To further expand upon these results, the role of lithium ion diffusion in the pause recovery must be better understood as well as polysulfide adsorption effects in the cathode, which play an important role in polysulfide mass transport away from the cathode.

Acknowledgements

This work was partly funded by the Battery 500 Seedling Program of the Energy Efficiency & Renewable (EERE) Office in the U.S. Department of Energy (DE-EE0008193).

References

[1] M.A. Hannan, M.M. Hoque, A. Mohamed, A. Ayob, Review of energy storage systems for electric vehicle applications: Issues and challenges, Renew. Sustain. Energy Rev. 69 (2017) 771–789. doi:10.1016/j.rser.2016.11.171.

[2] A. Manthiram, Y. Fu, S.-H. Chung, C. Zu, Y.-S. Su, Rechargeable Lithium–Sulfur Batteries, Chem. Rev. 114 (2014) 11751–11787. doi:10.1021/cr500062v.

[3] J. Liu, D. Lu, J. Zheng, P. Yan, B. Wang, X. Sun, Y. Shao, C. Wang, J. Xiao, J.G. Zhang, J. Liu, Minimizing Polysulfide Shuttle Effect in Lithium-Ion Sulfur Batteries by Anode Surface Passivation, ACS Appl. Mater. Interfaces. 10 (2018) 21965–21972. doi:10.1021/acsami.8b02381.

[4] Q. Wang, J. Jin, X. Wu, G. Ma, J. Yang, Z. Wen, A shuttle effect free lithium sulfur battery based on a hybrid electrolyte, Phys. Chem. Chem. Phys. 16 (2014) 21225–21229. doi:10.1039/c4cp03694h.

[5] M. Liu, Q. Li, X. Qin, G. Liang, W. Han, D. Zhou, Y.-B. He, B. Li, F. Kang, Suppressing Self-Discharge and Shuttle Effect of Lithium-Sulfur Batteries with V 2 O 5 -Decorated Carbon Nanofiber Interlayer, Small. 13 (2017) 1602539. doi:10.1002/smll.201602539.

[6] A.F. Hofmann, D.N. Fronczek, W.G. Bessler, Mechanistic modeling of polysulfide shuttle and capacity loss in lithium-sulfur batteries, J. Power Sources. 259 (2014) 300–310. doi:10.1016/j.jpowsour.2014.02.082.

[7] Y. V Mikhaylik, J.R. Akridge, Polysulfide Shuttle Study in the Li/S Battery System, J. Electrochem. Soc. 151 (2004) A1969. doi:10.1149/1.1806394.

[8] S. Liu, X. Hong, D. Wang, Y. Li, J. Xu, C. Zheng, K. Xie, Hollow carbon spheres with nanoporous shells and tailored chemical interfaces as sulfur host for long cycle life of lithium sulfur batteries, Electrochim. Acta. 279 (2018) 10–18. doi:10.1016/j.electacta.2018.05.029.

[9] D. Gueon, J.T. Hwang, S.B. Yang, E. Cho, K. Sohn, D.K. Yang, J.H. Moon, Spherical

Macroporous Carbon Nanotube Particles with Ultrahigh Sulfur Loading for Lithium-Sulfur Battery Cathodes, ACS Nano. 12 (2018) 226–233. doi:10.1021/acsnano.7b05869.

[10] D. Lu, Q. Li, J. Liu, J. Zheng, Y. Wang, S. Ferrara, J. Xiao, J.G. Zhang, J. Liu, Enabling High-Energy-Density Cathode for Lithium-Sulfur Batteries, ACS Appl. Mater. Interfaces. 10 (2018) 23094–23102. doi:10.1021/acsami.8b05166.

[11] X. He, J. Ren, L. Wang, W. Pu, C. Jiang, C. Wan, Expansion and shrinkage of the sulfur composite electrode in rechargeable lithium batteries, J. Power Sources. 190 (2009) 154–156. doi:10.1016/j.jpowsour.2008.07.034.

[12] K. Zhang, Q. Zhao, Z. Tao, J. Chen, Composite of sulfur impregnated in porous hollow carbon spheres as the cathode of Li-S batteries with high performance, Nano Res. 6 (2013) 38–46. doi:10.1007/s12274-012-0279-1.

[13] D.S. Wu, F. Shi, G. Zhou, C. Zu, C. Liu, K. Liu, Y. Liu, J. Wang, Y. Peng, Y. Cui, Quantitative investigation of polysulfide adsorption capability of candidate materials for Li-S batteries, Energy Storage Mater. 13 (2018) 241–246. doi:10.1016/j.ensm.2018.01.020.

[14] X.Q. Zhang, B. He, W.C. Li, A.H. Lu, Hollow carbon nanofibers with dynamic adjustable pore sizes and closed ends as hosts for high-rate lithium-sulfur battery cathodes, Nano Res. 11 (2018) 1238–1246. doi:10.1007/s12274-017-1737-6.

[15] J.Y. Song, Y.Y. Wang, C.C. Wan, Review of gel-type polymer electrolytes for lithium-ion batteries, J. Power Sources. 77 (1999) 183–197. http://www.oalib.com/references/9023829.

[16] X. Cheng, J. Pan, Y. Zhao, M. Liao, H. Peng, Gel Polymer Electrolytes for Electrochemical Energy Storage, Adv. Energy Mater. 8 (2018) 1–16. doi:10.1002/aenm.201702184.

[17] A.M. Stephan, Review on gel polymer electrolytes for lithium batteries, Eur. Polym. J. 42 (2006) 21–42. doi:10.1016/j.eurpolymj.2005.09.017.

[18] J.K. Kim, Hybrid gel polymer electrolyte for high-safety lithium-sulfur batteries, Mater. Lett. 187 (2017) 40–43. doi:10.1016/j.matlet.2016.10.069.

[19] A. Natarajan, A.M. Stephan, C.H. Chan, N. Kalarikkal, S. Thomas, Electrochemical studies on composite gel polymer electrolytes for lithium sulfur-batteries, J. Appl. Polym. Sci. 134 (2017) 1–8. doi:10.1002/app.44594.

[20] J. Chen, W.A. Henderson, H. Pan, B.R. Perdue, R. Cao, J.Z. Hu, C. Wan, K.S. Han, K.T. Mueller, J.G. Zhang, Y. Shao, J. Liu, Improving Lithium-Sulfur Battery Performance under Lean Electrolyte through Nanoscale Confinement in Soft Swellable Gels, Nano Lett. 17 (2017) 3061–3067. doi:10.1021/acs.nanolett.7b00417.

[21] M. Liu, D. Zhou, Y.B. He, Y. Fu, X. Qin, C. Miao, H. Du, B. Li, Q.H. Yang, Z. Lin, T.S. Zhao, F. Kang, Novel gel polymer electrolyte for high-performance lithium-sulfur batteries, Nano Energy. 22 (2016) 278–289. doi:10.1016/j.nanoen.2016.02.008.

[22] K. Kumaresan, Y. Mikhaylik, R.E. White, A Mathematical Model for a Lithium–Sulfur Cell, J. Electrochem. Soc. 155 (2008) A576. doi:10.1149/1.2937304.

[23] P. Andrei, C. Shen, J.P. Zheng, Theoretical and experimental analysis of precipitation and solubility effects in lithium-sulfur batteries, Electrochim. Acta. 284 (2018) 469–484. doi:10.1016/j.electacta.2018.07.045.

[24] T. Zhang, M. Marinescu, S. Walus, P. Kovacik, G.J. Offer, What Limits the Rate Capability of Li-S Batteries during Discharge: Charge Transfer or Mass Transfer?, J. Electrochem. Soc. 165 (2018) A6001–A6004. doi:10.1149/2.0011801jes.

[25] H. Pan, X. Wei, W.A. Henderson, Y. Shao, J. Chen, P. Bhattacharya, J. Xiao, J. Liu, On the Way Toward Understanding Solution Chemistry of Lithium Polysulfides for High Energy Li-S Redox Flow Batteries, Adv. Energy Mater. 5 (2015) 1–7. doi:10.1002/aenm.201500113.

[26] M.Z. Bazant, Theory of chemical kinetics and charge transfer based on nonequilibrium thermodynamics, Acc. Chem. Res. 46 (2013) 1144–1160. doi:10.1021/ar300145c.

[27] T. Danner, G. Zhu, A.F. Hofmann, A. Latz, Modeling of nano-structured cathodes for improved lithium-sulfur batteries, Electrochim. Acta. 184 (2015) 124–133. doi:10.1016/j.electacta.2015.09.143.

[28] L.R. Bard, Allen J.; Faulkner, Electrochemical Methods, 2004.

[29] V. Thangavel, K. Xue, Y. Mammeri, M. Quiroga, A. Mastouri, C. Guéry, P. Johansson, M. Morcrette, A.A. Franco, A Microstructurally Resolved Model for Li-S Batteries Assessing the Impact of the Cathode Design on the Discharge Performance, J. Electrochem. Soc. 163 (2016) A2817–A2829. doi:10.1149/2.0051614jes.

[30] B. Tjaden, S.J. Cooper, D.J. Brett, D. Kramer, P.R. Shearing, On the origin and application of the Bruggeman correlation for analysing transport phenomena in electrochemical systems, Curr. Opin. Chem. Eng. 12 (2016) 44–51. doi:10.1016/j.coche.2016.02.006.

[31] W. Halim, J.H. Lee, S.M. Park, R. Zhang, S. Sarkar, T. O'Neil, Y.C. Chiang, Y.L. Joo, Directly deposited binder-free sulfur electrode enabled by air-controlled electrospray process, ACS Appl. Energy Mater. 2 (2019) 678–686. doi:10.1021/acsaem.8b01694.

[32] J.H. Lee, J. Kang, S.W. Kim, W. Halim, M.W. Frey, Y.L. Joo, Effective Suppression of the Polysulfide Shuttle Effect in Lithium-Sulfur Batteries by Implementing rGO-PEDOT:PSS-Coated Separators via Air-Controlled Electrospray, ACS Omega. 3 (2018) 16465–16471. doi:10.1021/acsomega.8b02551.

[33] X. Tao, J. Wan, C. Liu, H. Wang, H. Yao, G. Zheng, Z.W. Seh, Q. Cai, W. Li, G. Zhou, C. Zu, Y. Cui, Balancing surface adsorption and diffusion of lithium-polysulfides on nonconductive oxides for lithium-sulfur battery design, Nat. Commun. 7 (2016) 1–9. doi:10.1038/ncomms11203.

[34] B.P. Williams, Y.L. Joo, Tunable Large Mesopores in Carbon Nanofiber Interlayers for High-Rate Lithium Sulfur Batteries, J. Electrochem. Soc. 163 (2016) A2745–A2756. doi:10.1149/2.0931613jes.

[35] J. Lee, B. Ko, J. Kang, Y. Chung, Y. Kim, W. Halim, J.H. Lee, Y.L. Joo, Facile and scalable fabrication of highly loaded sulfur cathodes and lithium–sulfur pouch cells via air-controlled electrospray, Mater. Today Energy. 6 (2017) 255–263. doi:10.1016/j.mtener.2017.11.003.

[36] J. Song, M.L. Gordin, T. Xu, S. Chen, Z. Yu, H. Sohn, J. Lu, Y. Ren, Y. Duan, D. Wang, Strong lithium polysulfide chemisorption on electroactive sites of nitrogen-doped carbon composites for high-performance lithium-sulfur battery cathodes, Angew. Chemie - Int. Ed. 54 (2015) 4325–4329. doi:10.1002/anie.201411109.

[37] S.H. Chung, A. Manthiram, A polyethylene glycol-supported microporous carbon coating as a polysulfide trap for utilizing pure sulfur cathodes in lithium-sulfur batteries, Adv. Mater. 26 (2014) 7352–7357. doi:10.1002/adma.201402893.

[38] T. Zhou, W. Lv, J. Li, G. Zhou, Y. Zhao, S. Fan, B. Liu, B. Li, F. Kang, Q.H. Yang, Twinborn TiO2-TiN heterostructures enabling smooth trapping-diffusion-conversion of polysulfides towards ultralong life lithium-sulfur batteries, Energy Environ. Sci. 10 (2017) 1694–1703. doi:10.1039/c7ee01430a.

[39] J. Liu, L. Yuan, K. Yuan, Z. Li, Z. Hao, J. Xiang, Y. Huang, SnO2 as a high-efficiency polysulfide trap in lithium-sulfur batteries, Nanoscale. 8 (2016) 13638–13645. doi:10.1039/c6nr02345b.

[40] Y.C. Lu, Q. He, H.A. Gasteiger, Probing the lithium-sulfur redox reactions: A rotating-ring disk electrode study, J. Phys. Chem. C. 118 (2014) 5733–5741. doi:10.1021/jp500382s.

[41] L.O. Valøen, J.N. Reimers, Transport Properties of LiPF6-Based Li-Ion Battery Electrolytes, J. Electrochem. Soc. 152 (2005) A882. doi:10.1149/1.1872737.

Tables

Reaction	Index *m*	k_m (mol m^{-2} s^{-1})	n_m	$U_{eq0,m}$ (V)	$K_{sp,m}$
$S_8^{(s)}$ to $S_8^{(l)}$	1	6.72[a]	0	-	1/19[27]
$S_8^{(l)}$ to S_8^{2-}	2	$2\cdot10^{-9}$,[a]	1	2.39 [a]	-
S_8^{2-} to S_6^{2-}	3	$2\cdot10^{-11}$,[a]	1	237 [a]	-
S_6^{2-} to S_4^{2-}	4	$5\cdot10^{-12}$,[a]	1	2.24 [a]	-

S_4^{2-} to S^{2-}	5	$5 \cdot 10^{-10}$,a	1	2.1 a	$1 \cdot 10^{-4}$[27]
S^{2-} to $Li_2S^{(s)}$	6	$1.2464 \cdot 10^{-4}$,a	0	-	-

Table 1. Reaction parameters k_m (reaction rate constant), n_m (electrons per reaction), $U_{eq0,m}$ (open circuit voltage at reference conditions), and $K_{sp,m}$ (solubility product). [a]Assumed parameters.

Species *i*	$D_{0,i}$ (m^2s^{-1})	M_i (kg mol^{-1})	ρ_i (kg m^{-3})	$c_{0,i}$ (mol m^{-3})	$\varepsilon_{0,i}$
S_8 (s)	0	0.2565 [27]	2070.4 [27]	-	0.2 a
S_8	$1 \cdot 10^{-9}$,a	-	-	17.0 a	-
S_8^{2-}	$2.6 \cdot 10^{-10}$ [40]	-	-	$1 \cdot 10^{-7}$,a	-
S_6^{2-}	$1.7 \cdot 10^{-10}$ [40]	-	-	$1 \cdot 10^{-7}$,a	-
S_4^{2-}	$1 \cdot 10^{-9}$ - $1 \cdot 10^{-13}$,a	-	-	0.02416 a	-
S^{2-}	$8.6 \cdot 10^{-11}$,a	-	-	$1 \cdot 10^{-9}$,a	-
Li_2S (s)	0	0.0459 [27]	1659.9 [27]	-	0.0001 a
Li^+	$4 \cdot 10^{-10}$,a	-	-	1000	-
A^-	$1.24 \cdot 10^{-10}$ [41]	-	-	1000	-

Table 2. Bulk diffusion coefficient ($D_{0,i}$), molecular weight (M_i), density (ρ_i), initial concentration ($c_{0,i}$), and initial volume fraction ($\varepsilon_{0,i}$) for molecular species in the model. [a]Assumed parameters.

Symbol		Value	Units
N	Total number of discretized segments	11	-
N (inner)	Number of segments in the outer cathode region	4	
N (outer)	Number of segments in the inner cathode region	4	
l_c	Length of cell	$6 \cdot 10^{-5}$,a	m
l_{io}	Distance between inner and outer regions	$1 \cdot 10^{-6}$,a	m
a_s (inner)	Specific surface area in the inner region	$3.6 \cdot 10^{8}$,a	m^2m^{-3}
a_s(outer)	Specific surface area in the outer region	$4 \cdot 10^{7}$,a	m^2m^{-3}
β (inner)	Bruggeman coefficient in the inner region	20 a	-
β (outer)	Bruggeman coefficient in the outer region	1.5[22]	-
ε_c	Carbon volume fraction in cell	0.2a	-

$c_{Li+,ref}$	Lithium ion reference concentration	1007.64[29]	mol m^{-3}
a_{mtl}	Mass transport limitation prefactor	$1.3 \cdot 10^{-14,a}$	m^6 mol^{-2}
b_{mtl}	Mass transport limitation exponential	5 [a]	-
R	Gas constant	8.314	J K^{-1} mol^{-1}
T	Temperature	298.15	K
F	Faraday constant	96485	A mol^{-1}

Table 3. Structural and miscellaneous parameters. [a]Assumed parameters.

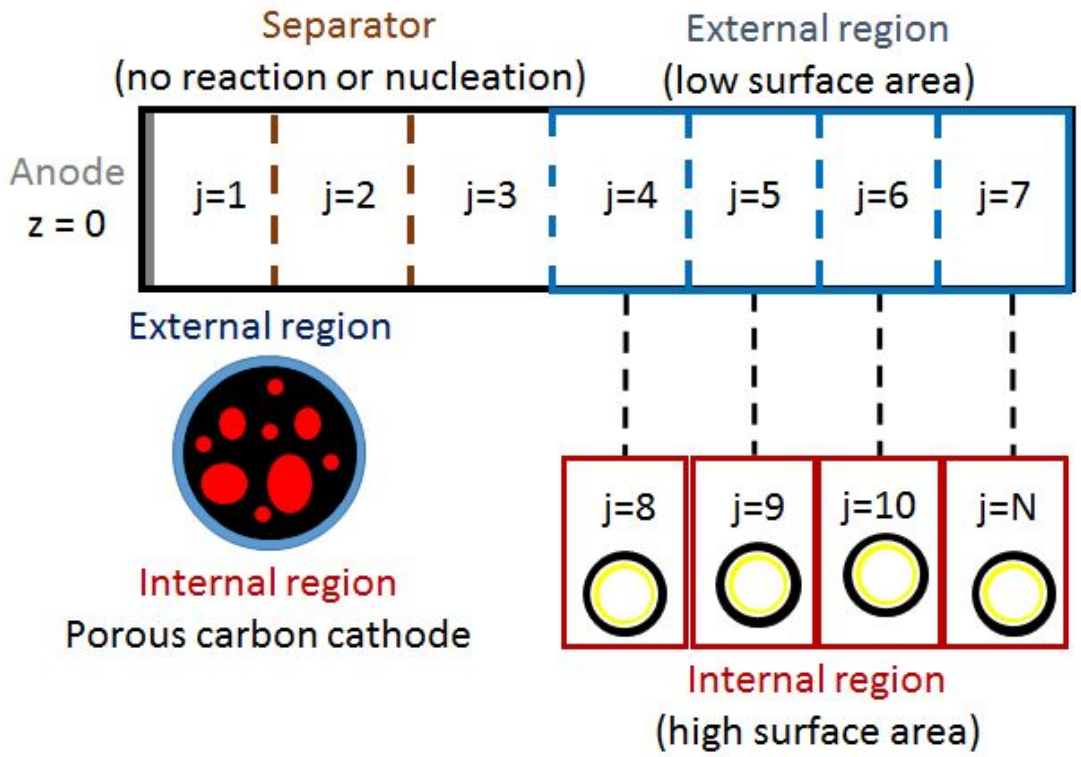

Fig. 1. Numerical discretization of a lithium-sulfur cell. The cathode was split into an inner and outer region corresponding to the inside and outside of spherical carbon cathode particles. Mass transport from inner regions only travels to the corresponding outer region.

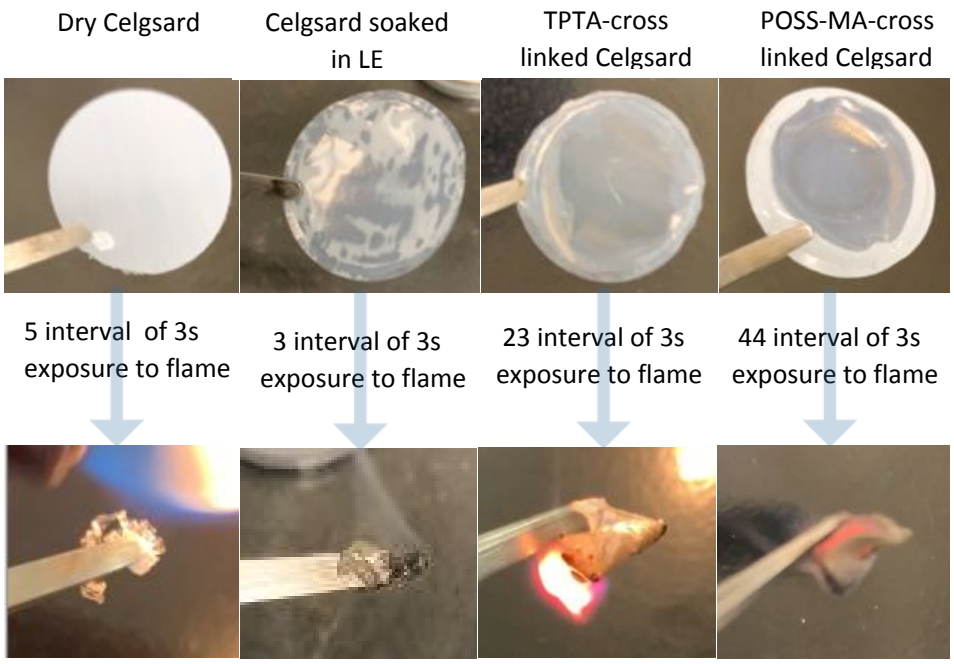

Fig. 2. Flammability test on Celgard, Celgard soaked in liquid electrolyte, TPTA-crosslinked Celgard (10%) and POSS-crosslinked Celgard (5%). The top and bottom row images are before and after the test.

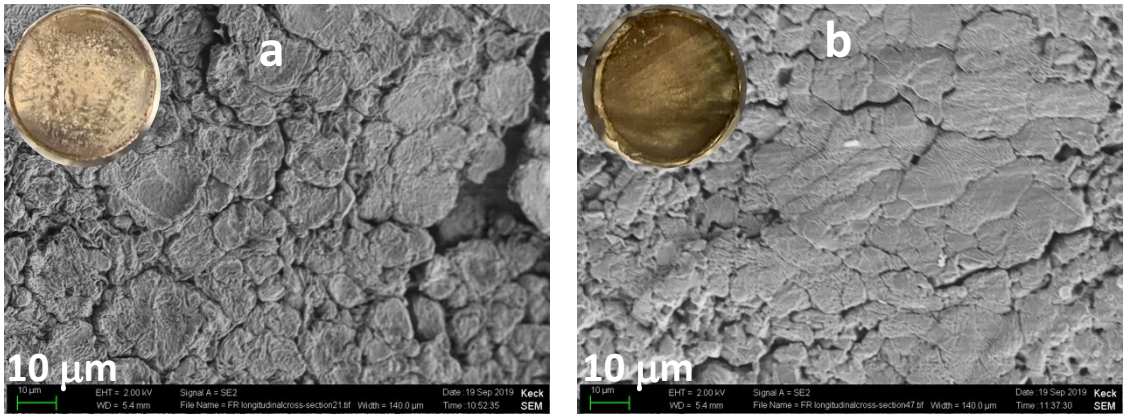

Fig. 3. SEM images of the Lithium surface in a) LE and b) GE battery after 100 cycling

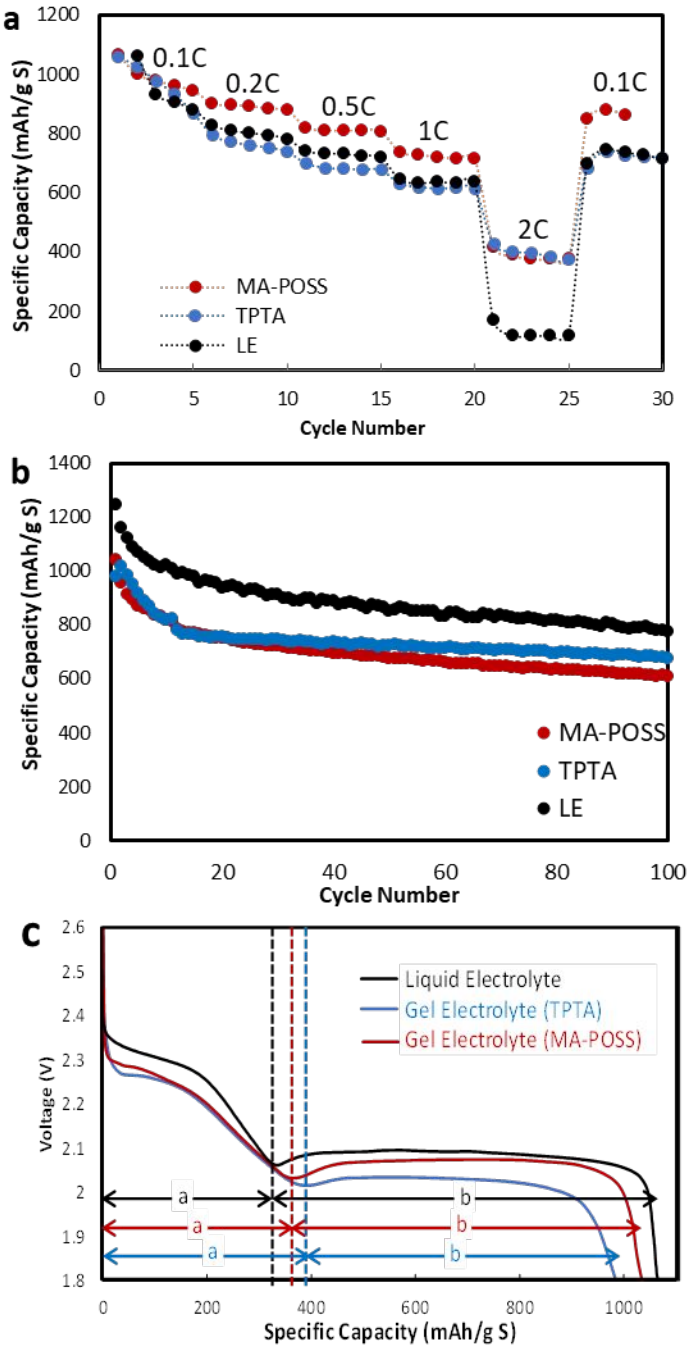

Fig. 4. a) Rate capability and, b) cycling performance, and c) first discharge curve of LE and GE batteries.

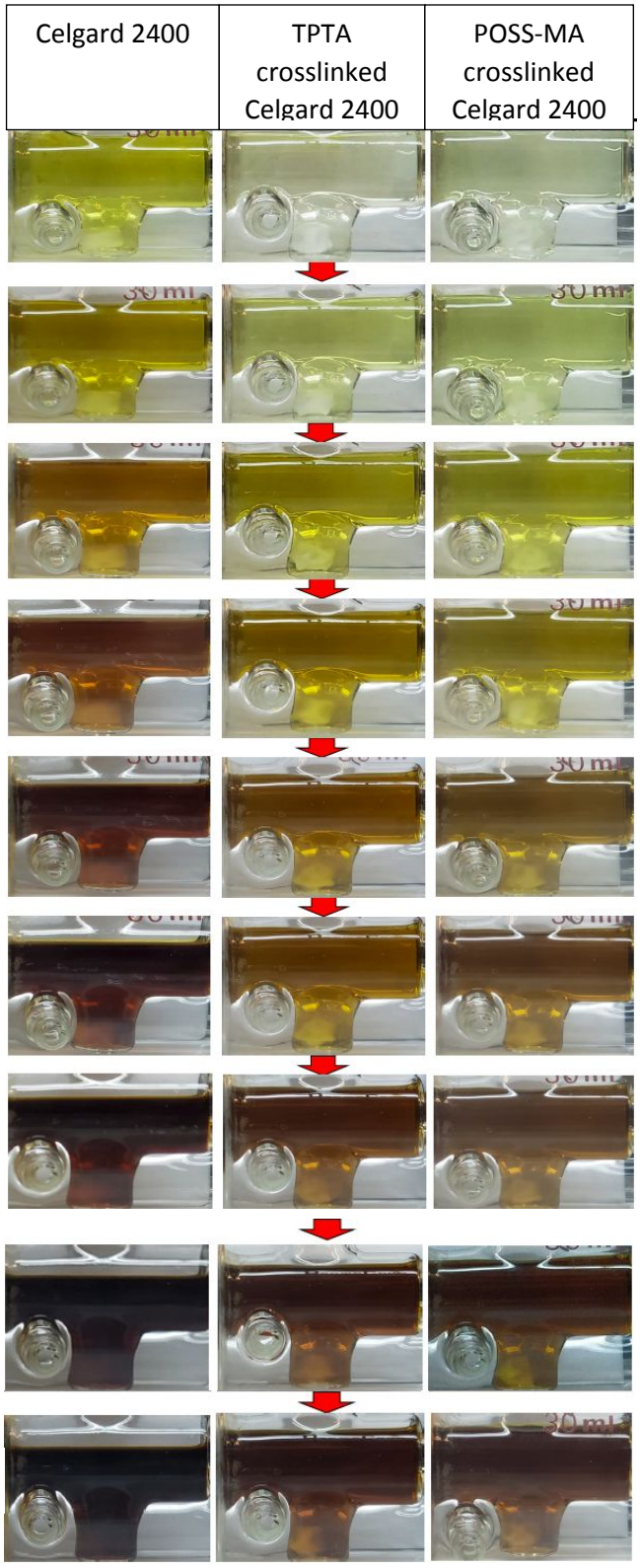

Fig. 5. Time lapse photos of diffusion of Li_2S_6 from the cathode chamber through the a) Celgard 2400, b) TPTA 10% crosslinked Celgard 2400 and c) POSS-MA 10% crosslinked Celgard 2400 separator towards the anode chamber.

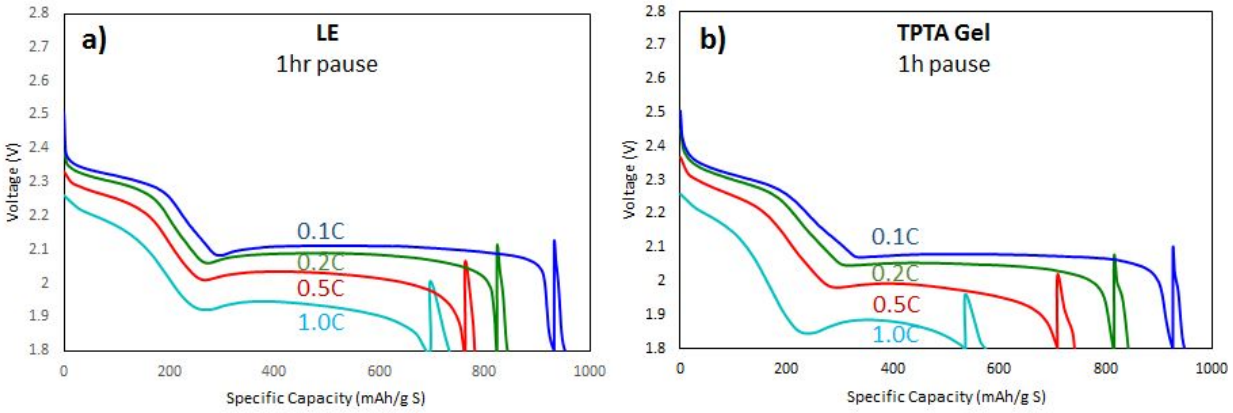

Fig. 6. Li-S coin cell discharge curves with pause for four discharge rates. (a) shows liquid electrolyte and (b) shows TPTA gel polymer electrolyte. The batteries were discharged normally to 1.8V, paused for 1hr, and then discharged again to 1.8V before charging normally.

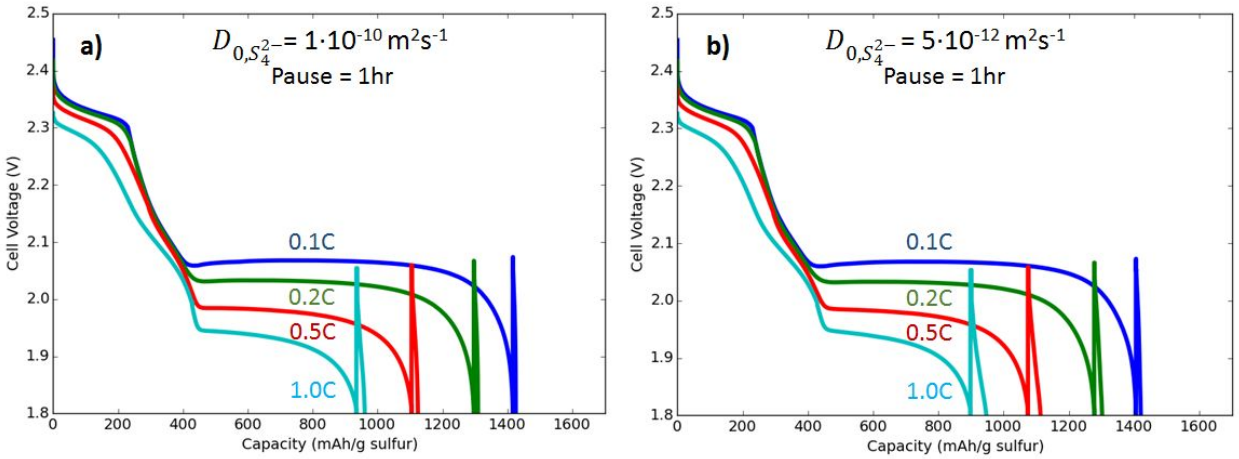

Fig. 7 Li-S numerical simulation discharge curves with 1 hr pause for four discharge rates. (a) shows the case of faster S_4^{2-} diffusion which and (b) shows slower S_4^{2-} diffusion.

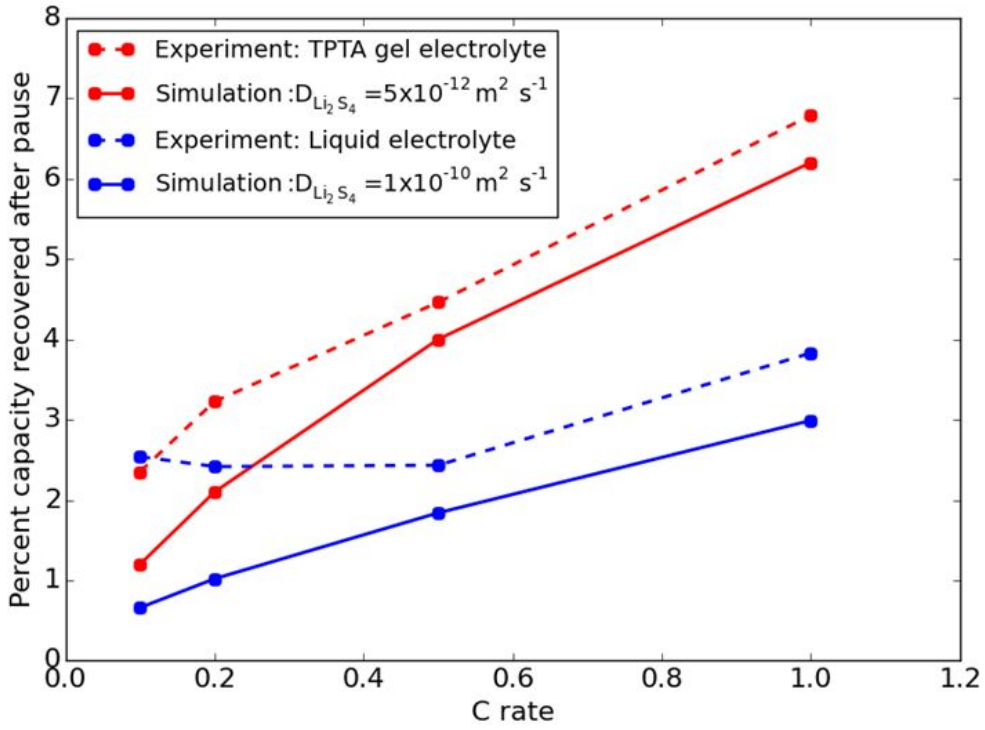

Fig. 8. Percent recoveries for 1 hour pause discharge for experiment and simulation. Percent recovery after pause was calculated by dividing the capacity gained after pause by the total capacity.

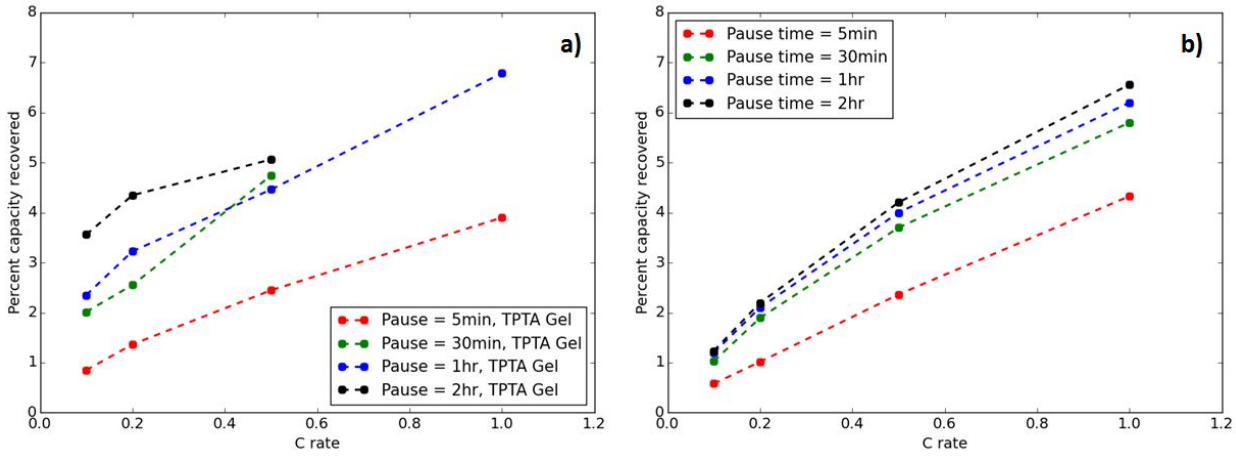

Fig. 9. Effect of pause time on percent capacity recovered after pause for experiment (a) and simulation (b). $D_{0,S_4^{2-}}$ = 5·10^{-12} m^{2}s^{-1} for the simulation results.

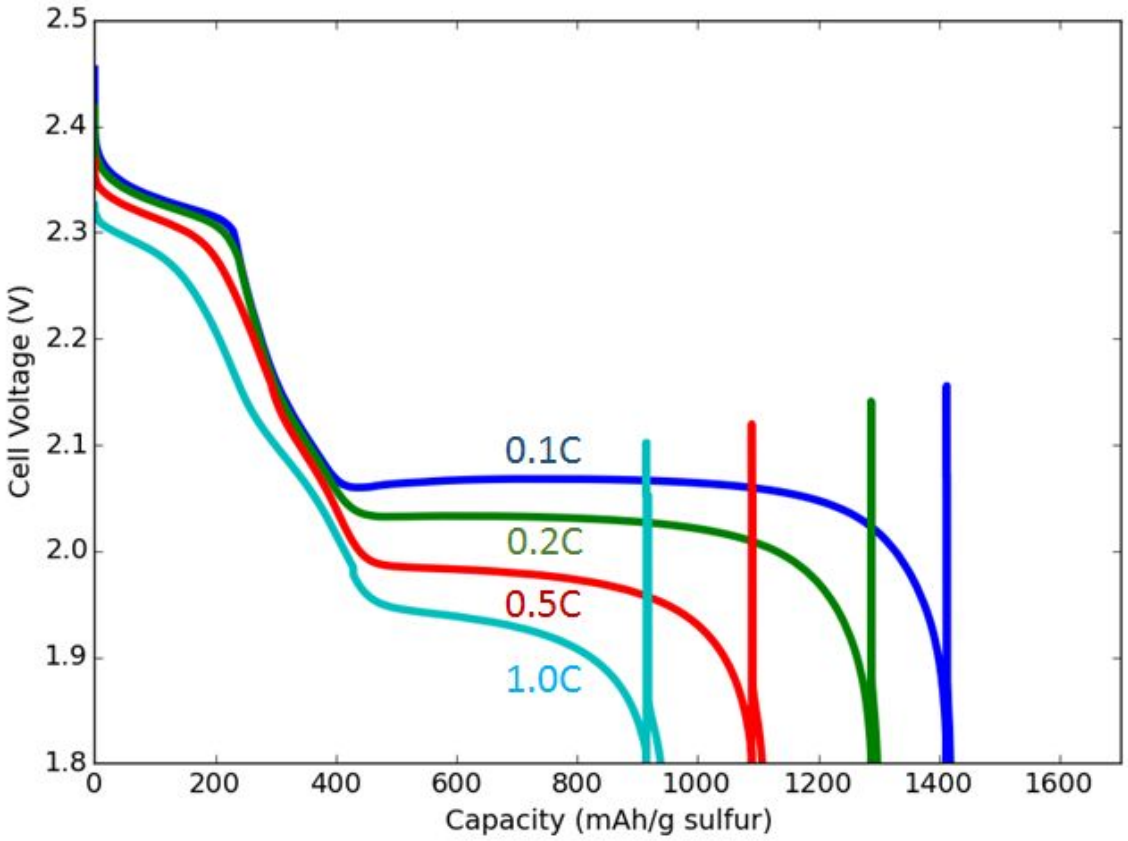

1

2 **Fig. 10.** Simulated discharge curves with S_6^{2-} reactions disabled after the 1 hour pause. The lower voltages
3 compared to Fig. 6a suggest that S_6^{2-} is still present at the end of discharge. $D_{0,S_4^{2-}} = 1 \cdot 10^{-11}$ m^{2}s^{-1}.